γ-ray spectroscopy of low-lying yrast and non-yrast states in neutron-rich ^{94,95,96}Kr

R.-B. Gerst,[1,*] A. Blazhev,[1] K. Moschner,[1] P. Doornenbal,[2] A. Obertelli,[2,3] K. Nomura,[4] J.-P. Ebran,[5,6] S. Hilaire,[5,6] J. Libert,[5,6] G. Authelet,[3] H. Baba,[2] D. Calvet,[3] F. Château,[3] S. Chen,[7,2] A. Corsi,[3] A. Delbart,[3] J.-M. Gheller,[3] A. Giganon,[3] A. Gillibert,[3] V. Lapoux,[3] T. Motobayashi,[2] M. Niikura,[8] N. Paul,[3,9] J.-Y. Roussé,[3,9] H. Sakurai,[2,8] C. Santamaria,[3] D. Steppenbeck,[2] R. Taniuchi,[2,8] T. Uesaka,[2] T. Ando,[2,8] T. Arici,[10] F. Browne,[11] A. M. Bruce,[11] R. Caroll,[12] L. X. Chung,[13] M. L. Cortés,[10,14] M. Dewald,[1] B. Ding,[15] F. Flavigny,[16,17] S. Franchoo,[16] M. Górska,[10] A. Gottardo,[16] J. Jolie,[1] A. Jungclaus,[18] J. Lee,[19] M. Lettmann,[14] B. D. Linh,[13] J. Liu,[19] Z. Liu,[15,20] C. Lizarazo,[10,14] S. Momiyama,[2,8] S. Nagamine,[2,8] N. Nakatsuka,[2,21] C. R. Nita,[22] C. Nobs,[11] L. Olivier,[16] R. Orlandi,[23] Z. Patel,[12] Zs. Podolyák,[12] M. Rudigier,[12] T. Saito,[2,8] C. Shand,[12] P.-A. Söderström,[2] I. Stefan,[16] V. Vaquero,[18] V. Werner,[14] K. Wimmer,[8] and Z. Xu[19]

[1]*Institut für Kernphysik, Universität zu Köln, 50937 Köln, Germany*
[2]*RIKEN Nishina Center, Wako, Saitama 351-0198, Japan*
[3]*IRFU, CEA, Université Paris-Saclay, 91191 Gif-sur-Yvette, France*
[4]*Department of Physics, Faculty of Science, University of Zagreb, HR-10000 Zagreb, Croatia*
[5]*CEA, DAM, DIF, F-91297 Arpajon, France*
[6]*Laboratoire Matière en Conditions Extrêmes, CEA, Université Paris-Saclay, 91680 Bruyères-le-Châtel, France*
[7]*School of Physics and State Key Laboratory of Nuclear Physics and Technology, Peking University, Beijing 100871, China*
[8]*Department of Physics, University of Tokyo, 7-3-1 Hongo, Bunkyo, Tokyo 113-0033, Japan*
[9]*Laboratoire Kastler Brossel, Sorbonne Université, CNRS, ENS-PSL Research University, Collège de France, Case 74, 4 Place Jussieu, F-75005 Paris, France*
[10]*GSI Helmholtzzentrum für Schwerionenforschung GmbH, 64291 Darmstadt, Germany*
[11]*School of Computing, Engineering and Mathematics, University of Brighton, Brighton BN2 4GJ, United Kingdom*
[12]*Department of Physics, University of Surrey, Guildford GU2 7XH, United Kingdom*
[13]*Institute for Nuclear Science and Technique, VINATOM, 179 Hoang Quoc Viet Road, Cau Giay, Hanoi, Vietnam*
[14]*Institut für Kernphysik, Technische Universität Darmstadt, 64289 Darmstadt, Germany*
[15]*Institute of Modern Physics, Chinese Academy of Sciences, Lanzhou 730000, China*
[16]*Institut de Physique Nucléaire, CNRS-IN2P3, Université Paris-Saclay, 91406 Orsay Cedex, France*
[17]*LPC Caen, CNRS/IN2P3, Normandie Université ENSICAEN, UNICAEN, 14000 Caen, France*
[18]*Instituto de Estructura de la Materia, CSIC, 28006 Madrid, Spain*
[19]*Department of Physics, The University of Hong Kong, Pokfulam 999077, Hong Kong, China*
[20]*School of Nuclear Science and Technology, University of Chinese Academy of Sciences, Beijing 100049, China*
[21]*Department of Physics, Faculty of Science, Kyoto University, Kyoto 606-8502, Japan*
[22]*Horia Hulubei National Institute of Physics and Nuclear Engineering (IFIN-HH), R-077125 Bucharest, Romania*
[23]*Advanced Science Research Center, Japan Atomic Energy Agency, Tokai, Ibaraki 319-1195, Japan*

We report on γ-ray spectroscopy of low-lying excited states in the neutron-rich ^{94,95,96}Kr isotopes measured as part of the "Shell Evolution And Search for Two-plus energies At RIBF" (SEASTAR) campaign at the RIKEN Radioactive Isotope Beam Factory. Excited yrast and non-yrast states were observed, and half-lives extracted via GEANT4 simulations. In ^{94,96}Kr candidates for the 3_1^- state were identified. For ^{95}Kr, the prompt SEASTAR data were combined with delayed spectroscopic data measured with the EURICA array to observe transitions on top of the known $(7/2)^+$ isomer at a level energy of 195.5(3) keV. The comparison of the new experimental results with five-dimensional collective Hamiltonian (5DCH) and mapped interacting boson model (IBM) calculations, both using the Gogny D1M interaction, could suggest oblate-prolate shape coexistence already in ^{96}Kr.

I. INTRODUCTION

Studying the changes of nuclear characteristics in dependence on the number of nucleons is highly important for our understanding of the forces that govern the atomic nucleus. Atomic nuclei in the close vicinity of the magic numbers for protons and neutrons show spherical shapes. The structure of one-particle (one-hole) neighbors of doubly-magic nuclei can be described by independently moving particles (holes) in a spherically symmetric potential created by an inert core. However, when moving away from the regions of doubly

*Corresponding author: rgerst@ikp.uni-koeln.de

magic nuclei, residual interactions between the valence nucleons become increasingly important. Already, nuclei with two protons or neutrons outside a closed shell exhibit a different structure than closed shell nuclei [1]. Adding more and more nucleons, the properties of nuclear excited states start to show features of collective motion, such as vibrational and rotational excitation modes related to the deformation of the nuclear shape. In some mass regions, this interaction between collective and single-particle—macroscopic and microscopic—degrees of freedom can lead to a very sudden increase of collectivity. Strontium and zirconium isotopes in the $A = 100$ region show a sudden onset of deformation at neutron number $N = 60$, while the lighter isotopes up to $N = 58$ are more spherical [2]. This transition belongs to the most dramatic shape changes in the nuclear chart and is accompanied by the appearance of low-lying 0_2^+ states [3,4].

This behavior can be explained by one spherical and one deformed configuration coexisting at low excitation energies. With increasing neutron number, one configuration suddenly becomes energetically favorable [2]. In even-even nuclei, this phenomenon is usually accompanied by a sudden drop of the $E(2_1^+)$ energy and the lowering of an excited 0^+ state [3,4]—the bandhead of the competing configuration. Experimentally, it has been shown that the isotopic chains of Sr, Zr, and Mo exhibit this very sudden onset of deformation going from $N = 58$ to $N = 60$ [5–10]. Experimental results from mass measurements of krypton and rubidium isotopes and from γ spectroscopy of ^{97}Rb established $Z = 37$ as the boundary of the $A = 100$ region of deformation with ^{97}Rb as the lower cornerstone of this phenomenon [11,12]. In addition, a rather smooth onset of deformation for krypton isotopes up to $N = 60$ with a gradual decrease in $E(2_1^+)$ has been determined from Coulomb excitation measurements at the REX-ISOLDE facility at CERN [13,14]. While this was reproduced in calculations using a proton-neutron interacting boson model (IBM-2) Hamiltonian based on the microscopic Gogny-D1M EDF [14], these mean-field calculations also suggested the existence of a second minimum in potential energy surfaces for ^{96}Kr, indicating the coexistence of an intruder structure of prolate deformed shape also for the krypton isotopic chain. Recent experimental results corroborated these theoretical predictions for $N \geqslant 60$ isotopes [15,16]. Measurements performed at GANIL revealed a very low $E(4_1^+)/E(2_1^+)$ ratio for ^{96}Kr, labeling Kr ($Z = 36$) as the new low-Z edge of the region [15]. Furthermore, the first measurements of excited states in ^{98,100}Kr showed a drop of $E(2_1^+)$ energies [16]. For ^{98}Kr, a low-lying $(0_2^+, 2_2^+)$ candidate was identified, providing experimental indication of a coexisting deformed configuration [16].

For the understanding of shape evolution in the krypton isotopic chain, various theoretical approaches have been used in recent years [14,17–21]. State-of-the-art beyond-self-consistent mean-field calculations on the krypton isotopic chain for mass 70 to 98 reproduced the general systematics over the large mass range [17], but underestimated the experimental $E(2_1^+)$ of ^{96}Kr, predicting a stronger shape phase transition at $N = 60$ than observed. The constraints of the (beyond-)mean-field calculations can be overcome by a microscopically based IBM calculation. The microscopically calculated potential energy surface (PES) in the β-γ plane is mapped onto the expectation value of the IBM Hamiltonian [22]. From this mapping procedure one can determine the parameters of the Hamiltonian of the IBM, which then enables the comparison with experimentally accessible spectroscopic observables sensitive to nuclear deformation, such as excitation energy ratios, quadrupole transition strength, and electromagnetic moments [22]. This technique was used to perform Gogny-D1M calculations to investigate the even-A krypton isotopes [18]. For $^{88–92}$Kr, this presents a defined γ softness that develops into a γ-soft oblate minimum for ^{94}Kr. For the isotopes with $N > 58$, the energy surfaces reveal a pronounced prolate-oblate shape coexistence.

II. EXPERIMENT

In this work, we report on new γ-ray spectroscopic information for the nuclei ^{94,95,96}Kr that was obtained from an experiment carried out at the Radioactive Isotope Beam Factory, operated by the RIKEN Nishina Center and the Center for Nuclear Study of the University of Tokyo. Radioactive isotope beams were produced via in-flight fission of a ^{238}U primary beam with an energy of 345 MeV/u and a mean intensity of 27 p nA on a 3 mm thick Be production target.

A schematic of the setup is depicted in Fig. 1. The isotopes of interest were selected and separated with the $B\rho$-ΔE-$B\rho$ method in the fragment separator BigRIPS [23]. A clean event-by-event identification of the secondary beam was obtained via a TOF-$B\rho$-ΔE measurement [24]. Plastic scintillators were used to measure the time-of-flight (TOF), parallel plate avalanche counters (PPACs) to determine $B\rho$, and a multiple sampling ionization chamber (MUSIC) to deduce the energy loss ΔE and consequently Z. Secondary reactions took place on a 99(1) mm thick [725(7) mg/cm^2] liquid hydrogen target surrounded by a 300 mm long cylindrical time projection chamber (TPC) forming the system MINOS [25]. Reaction residues after the target had an average energy of $\approx$ 180 MeV/nucleon and were identified by the ZeroDegree [23] spectrometer using techniques similar to those described for BigRIPS. In Fig. 2, the particle identification plots obtained with this method for (a) BigRIPS and (b) ZeroDegree are shown. The data presented in this work were collected during 35 hours, 33 hours with the transmission through BigRIPS optimized for ^{95}Br and through ZeroDegree for ^{94}Se, and an additional two hours with ZeroDegree centered on ^{95}Kr. The use of MINOS allowed for the tracking of ejected charged particles—protons—and therefore for a reconstruction of the reaction vertex. This was required due to the dimensions of the liquid hydrogen target, and allowed for a more precise determination of the projectile velocity and emission angle of γ rays needed for the Doppler correction of the detected γ-ray energies. The reaction vertex was reconstructed either from two outgoing protons or from one proton and the beam particle whose position was measured with two upstream PPACs. The detection efficiency of at least one proton was simulated at 95% with a vertex position resolution of 5 mm (FWHM) along the beam axis [25]. Deexciting γ rays from states in ^{94}Kr, ^{95}Kr, and ^{96}Kr were detected by the DALI2

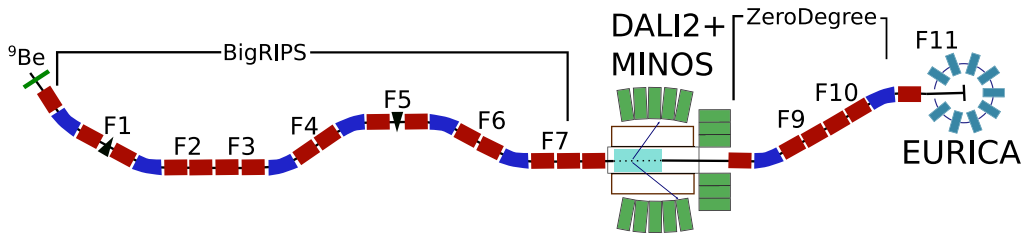

FIG. 1. Schematic of the experimental setup including the BigRIPS fragment separator, MINOS target system, DALI2 array, ZeroDegree spectrometer, and EURICA array (see text for details). Quadrupole magnets are shown in red, dipole magnets in blue. At F1 and F5, degraders are depicted in black. Plastic scintillators and parallel plate avalanche counters were placed at several focal planes. Figure adapted from [23].

high-efficiency γ-ray spectrometer [26], comprising 186 NaI(Tl) detectors. Energy calibrations were performed using ^{60}Co, ^{137}Cs, ^{88}Y, and ^{133}Ba sources, resulting in a calibration error of 3 keV in the range 350–1300 keV and an energy resolution of 9% (6%) FWHM at 662 keV (1.33 MeV). Using addback when the centers of hit detectors were less than 15 cm apart, the full-energy peak γ-ray detection efficiency was simulated with the GEANT4 toolkit [27] to be 35% (23%) for 500 keV (1 MeV) γ rays emitted in flight. With this setup, transition energies can be determined by fitting the simulated response functions together with a double-exponential background to the γ-spectra of the different reaction channels. However, the lifetimes of excited states influence the Doppler shift of the γ-ray energies and need to be considered when using this approach. The known energies and lifetimes of the 2_1^+ states in ^{94}Kr and ^{96}Kr were used as a proof of concept, yielding consistent results with literature [13,14]. The tertiary

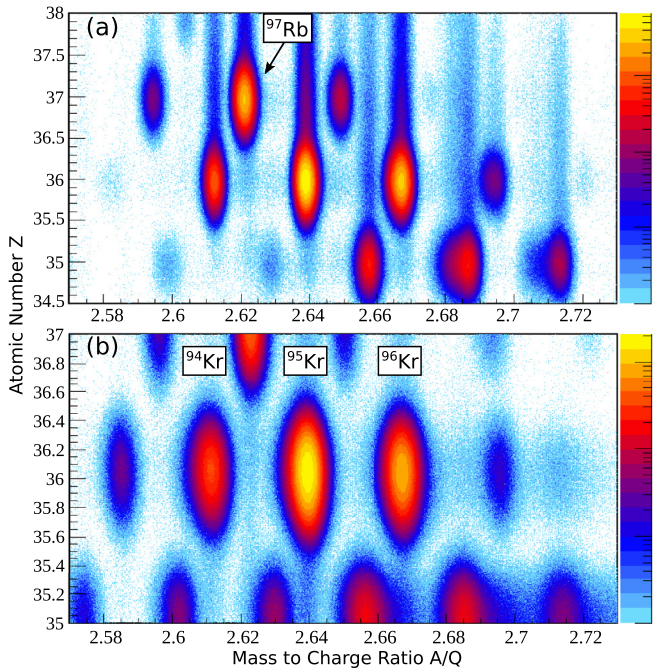

FIG. 2. Particle identification plots for (a) BigRIPS and (b) ZeroDegree spectrometer. The secondary beam in front of the reaction target and reaction residues are labeled and clearly separated. See text for details.

beam particles were delivered via the ZeroDegree spectrometer to the Euroball RIKEN Cluster Array (EURICA) [28], where the beam was stopped in the center. With this high resolution γ-ray spectrometer consisting of twelve high-purity germanium cluster detectors, it was possible to measure long-lived isomers, such as the known one in ^{95}Kr [29]. Similar to DALI2, an addback analysis was performed. The peak-to-total ratio of a full energy peak at 1333 keV after addback was 25.8% with an energy resolution of 3.17 keV [28]. This setup enabled a prompt-delayed correlation analysis of conjoined data from SEASTAR (Shell Evolution And Search for Two-plus energies At RIBF) and EURICA, and made it possible to identify the prompt γ rays as either feeding or bypassing the known isomeric state in ^{95}Kr.

III. DATA ANALYSIS AND RESULTS

A. ^{94}Kr

Until recently, the only published γ transitions in ^{94}Kr were those at 665.5, 853.2, and 1001.3 keV, measured via Coulomb excitation at the REX-ISOLDE facility [13] and following spontaneous fission of ^{248}Cm with the EUROGAM 2 array [30]. On the basis of angular correlation analysis, spin and parity of 2^+ and of 4^+ were assigned to the levels at 665.5 and 1518.7 keV, respectively, with the remaining transition of 1001.3 keV populating the 4^+ level [30].

Very recently, this level scheme was expanded upon using prompt and delayed γ-ray spectroscopy data measured using the novel hybrid spectrometer ν-Ball during the fission campaign at the ALTO facility of IPN Orsay [31–33]. Additionally, a short-lived 32(3) ns isomer at 3444 keV was discovered [33]. With a flight time of 240 ns through the ZeroDegree spectrometer, even if populated, this isomer is not expected to be observed with EURICA. At the same time its half-life is too long to be seen with DALI2, where only γ transitions with half-lives up to $\approx$ 1 ns can be measured. In the present experiment, excited states in ^{94}Kr were mainly populated via the ^{95}Kr$(p, pn)^{94}$Kr knockout and the ^{94}Kr$(p, p')^{94}$Kr inelastic scattering reactions. The first excited 2^+ state of ^{94}Kr is known to have a half-life of $8.7^{+1.0}_{-0.8}$ ps [14]. When Doppler correction is performed with the reconstructed vertices of the reaction points, the measured γ-ray lines are shifted to smaller energies compared to the transition energy. Therefore, estimates for lifetimes of excited states can be made by comparing the experimental line shapes with GEANT4 Monte Carlo simulations, as demonstrated in [34,35].

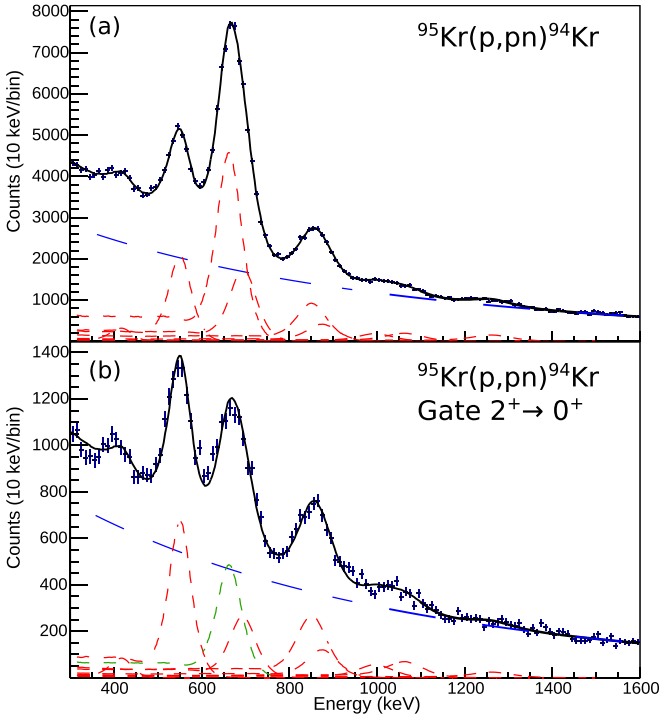

FIG. 3. Doppler-corrected γ-ray energy spectra of DALI2 in prompt coincidence with the ^{95}Kr(p, pn) ^{94}Kr reaction channel. The spectra were fitted with simulated response functions (red) and a two-component exponential background (blue dashed curve). (a) Full spectrum with γ multiplicity $M_\gamma < 6$. (b) Spectrum gated on the 2_1^+ to 0_1^+ 665.5 keV transition (marked in green) without background subtraction.

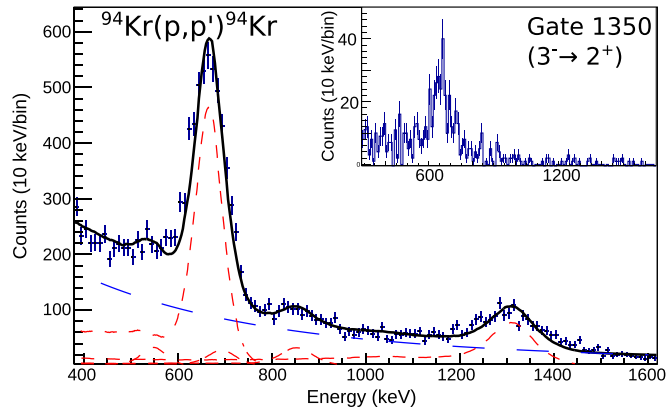

FIG. 4. Doppler corrected γ-ray spectrum measured with DALI2 for the ^{94}Kr(p, p') ^{94}Kr reaction channel. The spectrum was fitted with simulated response functions (red) and a two-component exponential background (blue dashed curve). The inset shows part of the spectrum gated on the newly observed 1350(38) keV transition with background subtraction.

The uncertainties of newly determined transition energies are dominated by the systematic error from these lifetime effects. The error was determined from χ^2 profiles of different energy-lifetime combinations. The final uncertainties also include a statistical contribution from the fitting procedure and the calibration error. Doppler-corrected spectra for ^{94}Kr populated in the ^{95}Kr(p, pn) ^{94}Kr reaction are presented in Fig. 3. In order to obtain the energies of the identified transitions, the spectrum was least-squares fitted with simulated response functions of the DALI2 array and a two-component exponential background.

Figure 3(a) shows the full spectrum for a γ multiplicity $M_\gamma < 6$. In addition to the 551.2(2), 665.5(1), 695.3(2), 853.8(1), 1001.8(1) and 1267.1(2) keV transitions, already known [13,30,33], the spectrum exhibits three so far unobserved lines at 428(17), 880^{+22}_{-17}, and 1083^{+29}_{-27} keV. Figure 3(b) shows a γ-γ coincidence spectrum gated on the $2_1^+ \rightarrow 0_1^+$ transition without background subtraction. This spectrum was fitted with the same response functions as in the case of the full spectrum shown in Fig. 3(a). The intensities of all transitions are enhanced with this gate, with the strongest coincidence being the 551.2 and 853.8 keV transitions known to be in direct coincidence with the $2_1^+ \rightarrow 0_1^+$ transition. When looking only at multiplicity $M_\gamma = 1$ events, no transitions are enhanced in comparison to the full fit. Therefore, one can assume that the transitions not placed in the level scheme (see Fig. 5) are not ground state transitions.

As described above, half-life estimates can be determined via the GEANT4 aided data analysis based on the line shape of the γ transition which is affected by the decay half-life.

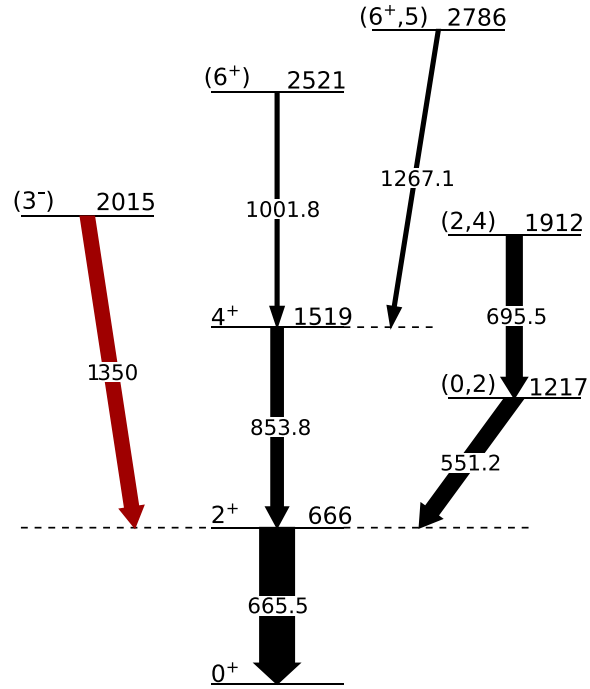

FIG. 5. Level scheme constructed for ^{94}Kr based on observed transitions in this work. Energies are given in keV. The widths of the transition arrows correspond to their observed efficiency-corrected intensities normalized to the strongest transition. The newly placed 1350(38) keV transition is shown in red (see Fig. 4). In addition, transitions with energies 428(17), 880^{+22}_{-17}, and 1083^{+29}_{-27} keV were observed, showing increased intensities when gating on the $2_1^+ \rightarrow 0_1^+$ transition, but could not be placed in the level scheme.

From this analysis, a half-life of $10.5^{+2.6}_{-2.0}$ ps was obtained for the 665.5 keV 2^+_1 level, in agreement with the literature value of $8.7^{+1.0}_{-0.8}$ ps [13]. Figure 4 shows the Doppler-corrected spectrum for ^{94}Kr populated in the ^{94}Kr$(p, p')^{94}$Kr inelastic scattering reaction. Next to the 551.2, 665.5, 695.3, and 853.8 keV transitions, an additional line at 1350(38) keV is included in the fit. Due to the reaction mechanism, the cross section for octupole collective excitations is enhanced [36–39]. Therefore, this is tentatively assigned as depopulating a (3^-) state with an energy of 2015(38) keV, as denoted in Fig. 5, where the proposed level scheme for ^{94}Kr is shown. The widths of the transition arrows correspond to measured efficiency-corrected intensities normalized to the strongest transition. Only transitions seen in coincidence with at least one other transition are placed in the level scheme. Even though the relative intensities of the 428(17), 880^{+22}_{-17}, and 1083^{+29}_{-27} keV transitions were enhanced when gating on the $2^+_1 \rightarrow 0^+_1$ transitions, they could not be placed in the level scheme.

B. ^{96}Kr

Doppler-corrected γ-ray energy spectra for ^{96}Kr populated in the ^{97}Rb$(p, 2p)^{96}$Kr reaction are presented in Fig. 6. As above, the spectrum was least-squares fitted with simulated response functions of the DALI2 array and a two-component exponential background.

The most intense transition at 554 keV in the γ-ray energy spectrum shown in panel (a) of Fig. 6 confirms the energy of the previously reported $(2^+_1) \rightarrow 0^+_1$ transition at 554.1(5) keV [13–15]. The spectrum also shows the rather strong line of 621(2) keV, which was tentatively assigned as the $(4^+_1) \rightarrow (2^+_1)$ transition in Ref. [15], and the line at 515(2) keV, as also seen in Ref. [15]. Additionally, the γ-ray spectrum of ^{96}Kr exhibits multiple so far unobserved transitions at 334(16), 819^{+22}_{-24}, 887^{+24}_{-23}, and 1185^{+36}_{-28} keV. Figure 6(c) shows a γ-γ coincidence spectrum gated on the $(2^+_1) \rightarrow 0^+_1$ transition. This spectrum was fitted with the same response functions as in the case of the total spectrum shown in Fig. 6(a). The lines at 334, 621, and 819 keV show clearly enhanced intensities in this fit. Therefore, in the proposed level scheme shown in Fig. 8, they are placed in direct coincidence with the $(2^+_1) \rightarrow 0^+_1$ transition.

The energy of the 1185 keV transition matches within the experimental errors the sum of energies of the $(4^+_1) \rightarrow (2^+_1)$ and $(2^+_1) \rightarrow 0^+_1$ transitions. However, this transition can be observed in coincidence with both of the former lines, which proves that the 1185 keV transition is not a sum line. In fact, the observation of the coincidence with the $(4^+_1) \rightarrow (2^+_1)$ makes this transition a possible candidate for the $(6^+_1) \rightarrow (4^+_1)$ transition, and thus we place a tentative (6^+) level with an energy of 2360^{+36}_{-28} keV. The placement of the non-yrast (2^+_2) state at an energy of 888(16) keV as shown in Fig. 8 is supported by the strong coincidence of the $(2^+_2) \rightarrow (2^+_1)$ transition of 334 keV with the $(2^+_1) \rightarrow 0^+_1$ transition. It also matches within errors the energy of the proposed ground state $(2^+_2) \rightarrow 0^+_1$ transition of 887 keV. Figure 6(b) shows a γ-ray spectrum where a γ multiplicity $M_\gamma = 1$ was demanded. Applying this condition, ground state transitions

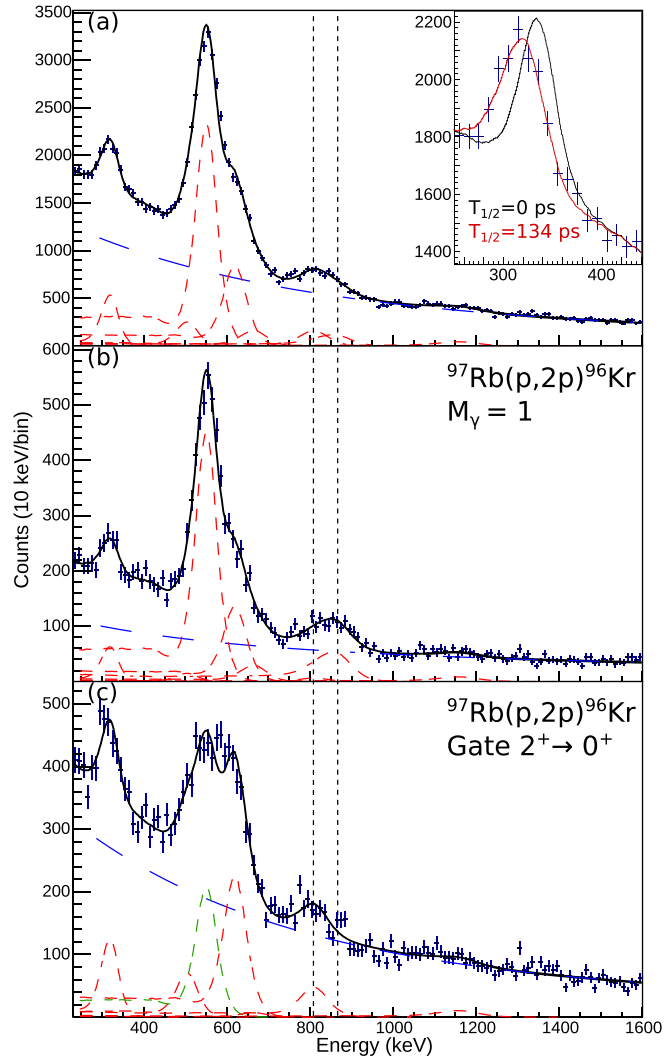

FIG. 6. Doppler corrected γ-ray energy spectra measured with DALI2 for the ^{97}Rb$(p, 2p)^{96}$Kr reaction channel. The spectra were fitted with simulated response functions (red) and a two-component exponential background (blue dashed curve). (a) Full spectrum with γ multiplicity $M_\gamma < 6$. The inset shows the comparison between the experimental shape of the 334 keV transition, assuming a half-life of 0 ps (black) and 134 ps (red) of the proposed 888(16) keV state. (b) Spectrum with $M_\gamma = 1$. (c) Gated on the (2^+_1) to 0^+_1 transition (green peak) without background subtraction. The dashed vertical lines in the three spectra denote the 819 and 887 keV γ transitions. While the former is enhanced by a gate on the (2^+_1) to 0^+_1 transition [see (c)], the latter is stronger in the $M_\gamma = 1$ spectrum.

from directly populated states appear enhanced compared to transitions which only occur within cascades. In Figure 6(b) this enhancement is observed only for the lines at 554 and 887 keV. A half-life estimate could be extracted for the level at 888 keV via line-shape analysis of the 334 [see inset of Fig. 6(a)] and 887 keV transitions depopulating the (2^+_2) state. This yielded 134^{+21}_{-27} and 122^{+71}_{-41} ps, respectively. The positions in the level scheme of the 515 and 819 keV transitions also remain unclear in the present study. Due to the strong coincidence of the 819 keV line with the $(2^+_1) \rightarrow 0^+_1$ transition,

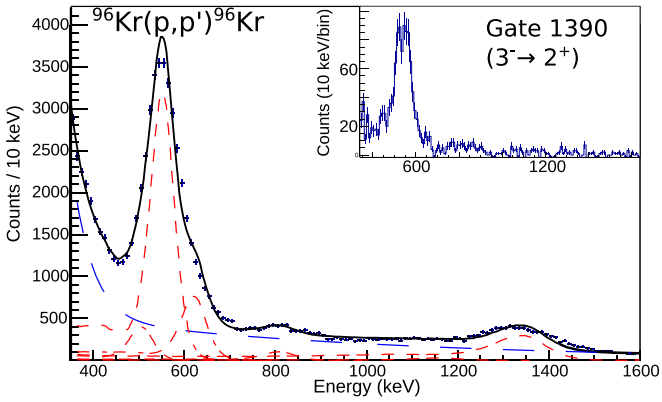

FIG. 7. Doppler corrected γ-ray energy spectrum measured with DALI2 for the ^{96}Kr(p, p')^{96}Kr reaction channel. The spectrum was fitted with simulated response functions (red) and a two-component exponential background (blue dashed curve). The inset shows part of the spectrum gated on the newly observed 1390(36) keV transition with background subtraction.

we propose the tentative placement of a state at 1373^{+22}_{-24} keV with undetermined spin and parity. The Doppler-corrected spectrum for ^{96}Kr populated in the ^{96}Kr(p, p')^{96}Kr reaction is presented in Fig. 7. Next to the $(2^+_1) \rightarrow 0^+_1$, $(4^+_1) \rightarrow (2^+_1)$ and the 515 and 819 keV transitions, it also contains a new 1390(36) keV transition. Similarly to ^{94}Kr, this observation indicates the enhanced cross-section for octupole collective excitations in the inelastic channel. The level scheme shown

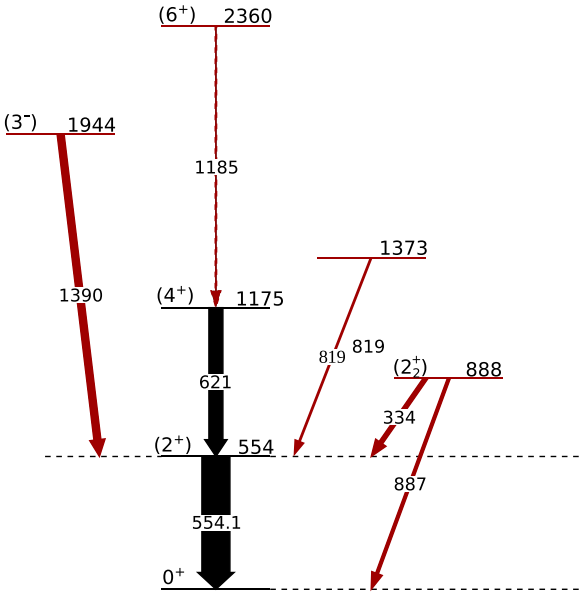

FIG. 8. Level scheme constructed for ^{96}Kr. Energies are given in keV. The widths of the transitions arrows correspond to their observed efficiency-corrected intensities normalized to the strongest transition. Newly placed transitions are shown in red (see Fig. 7). In addition, the 515 keV transition was observed in coincidence with the $2^+_1 \rightarrow 0^+_1$ transition, but could not be placed in the level scheme. (see text for details)

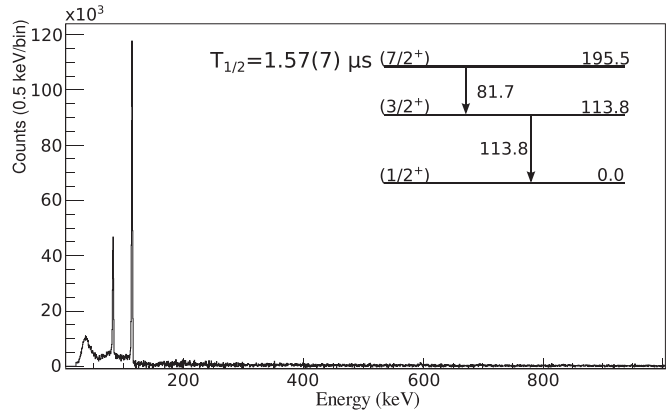

FIG. 9. Background-subtracted EURICA energy spectrum with a gate on ^{95}Kr in the ZeroDegree PID. The two peaks correspond to the two delayed transitions in ^{95}Kr at 81.7(2) and 113.8(2) keV depopulating the known $(7/2)^+$ isomer [29,40] as shown in the inset of the figure (see text for details).

in Fig. 8 therefore shows a newly determined (3^-_1) state at an energy of 1944(36) keV.

C. ^{95}Kr

Prior to this work, the only published γ transitions in ^{95}Kr were 81.7 and 113.8 keV below a long-lived isomeric level at 195.5(3) keV with a half-life of 1.4(2) µs first measured at the ILL reactor in Grenoble [29], and later confirmed at RIBF with an isomeric half-life of 1.582(22) µs [40].

A spin sequence of $(1/2)^+_{g.s.}$, $(3/2)^+$, $(7/2)^+$ was tentatively assigned due to the similarity in nuclear structure to the neighboring isotones ^{97}Sr and ^{99}Zr. Due to this similarity and the large difference in intensities of the two observed transitions, based on the different electron conversion coefficients, the multipolarities $M1$ for the 113.8(2) keV and $E2$ for the 81.7(2) keV transition were assigned [29]. In the present analysis of ^{95}Kr, one goal was to search for other isomeric decays ($T_{1/2} \gtrsim 100$ ns), shorter than 1.4 µs, but long enough to survive the flight through the ZeroDegree spectrometer ≈240 ns. Figure 9 shows the background-subtracted delayed γ spectrum correlated with ^{95}Kr ions arriving at F11 (see Fig. 1) taken by the high-resolution array EURICA. The transitions below the known $(7/2)^+$ isomer are clearly visible, while no further transitions are present. In this work, the half-life of the known isomeric level was determined as 1.57(7) µs in agreement with literature values [29,40]. The second, equally important goal was to observe coincidences between the known isomeric transitions, measured with EURICA, and prompt transitions, measured with DALI2. These two data sets were merged.

The isotope was populated via the ^{96}Kr(p, pn)^{95}Kr and ^{97}Rb(p, $2pn$)^{95}Kr nucleon knockout reactions. In Fig. 10, the DALI2 prompt Doppler-corrected γ-ray energy spectra for the (p, $2pn$) (a) and the (p, pn) (b) reaction channels are shown. The (p, p') inelastic reaction channel contains a very high background, and the analysis of the unmerged prompt data in this channel did not yield any conclusive results.

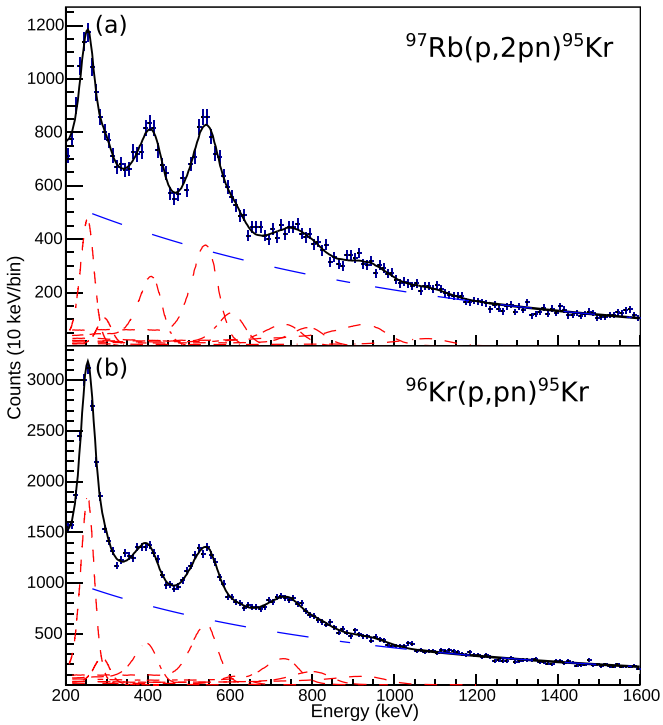

FIG. 10. Doppler-corrected γ-ray energy spectra measured with DALI2 for the two-nucleon removal and one-neutron knockout reaction channels ^{97}Rb$(p, 2pn)^{95}$Kr and ^{96}Kr$(p, pn)^{95}$Kr. The spectra were fitted with simulated response functions (red) and a two-component exponential background (blue dashed curve).

The full Doppler-corrected γ-ray energy spectra were simulated with GEANT4 as described before. The resulting energies and half-lives of the simulated response functions are shown in Table I. Due to the density of transitions observed for this even-odd isotope and the statistics, it was not possible to build a level scheme. It is noticeable, however, that even though both spectra were fitted with roughly the same response functions, the intensities vary depending on the reaction channel. This could be linked to the different nature of the excited levels. While for the (p, pn) reaction channel neutron excitations probably dominate, for the $(p, 2pn)$ reaction neutron and proton excitations are expected more equally. In a very simplified way, one could deduce that the transition at 260 keV, which has a higher intensity for the (p, pn) reaction, is related to excited neutron states. Another factor may be the nuclear structure of the incoming nuclei. ^{96}Kr in its ground state can be considered as oblately deformed (see Ref. [13] and discussion in Sec. IV A), while ^{97}Rb already has a stronger and prolate deformation [12].

TABLE I. Energies and half-life estimates of the response functions used to simulate the prompt spectra for the ^{97}Rb$(p, 2pn)^{95}$Kr and ^{96}Kr$(p, pn)^{95}$Kr reaction channels. Note that only effective half-lives can be extracted with this analysis. As above, the efficiency-corrected intensities are normalized to the strongest transition.

^{97}Rb $\rightarrow$ ^{95}Kr			^{96}Kr $\rightarrow$ ^{95}Kr		
E (keV)	$T_{1/2}$ (ps)	I_{rel}	E (keV)	$T_{1/2}$ (ps)	I_{rel}
260(16)	78^{+16}_{-13}	54(3)	260(16)	73(10)	100
300(19)	47^{+53}_{-37}	12(2)	299(19)	103^{+43}_{-34}	13(1)
430(23)	183^{+23}_{-26}	54(3)	421(24)	221^{+28}_{-34}	40(2)
561(23)	118^{+13}_{-16}	100	561(23)	123^{+12}_{-17}	75(2)
622^{+20}_{-21}	88^{+24}_{-52}	34(3)	629^{+25}_{-28}	$\leqslant$200	81(2)
769^{+30}_{-29}	184^{+97}_{-45}	36(4)	762(26)	143^{+33}_{-29}	51(2)
817^{+24}_{-32}	103^{+30}_{-90}	28(4)	839^{+23}_{-24}	172^{+68}_{-59}	30(2)
989^{+32}_{-34}	325^{+74}_{-85}	60(4)	989^{+36}_{-34}	378^{+138}_{-101}	32(2)
1123^{+39}_{-41}	146^{+129}_{-109}	19(3)			

To identify states on top of the isomer, e.g., in coincidence, we gate on the two isomeric transitions measured with EURICA in the merged data. The isomer gate used in the following is defined by requiring a coincidence with delayed γ rays registered in EURICA in the ranges 112.5–115.1 keV or 80.4–83.0 keV which represent the known 113.8 and 81.7 keV transitions depopulating the $(7/2)^+$ isomer in ^{95}Kr. The corresponding Doppler-corrected prompt DALI2 energy spectrum is filled with the events matched to the EURICA events by the merging process. The analysis is done for each reaction channel separately. In Fig. 11, the resulting three spectra for the three reaction channels are shown. The 561 and 989 keV transitions already seen in the ungated prompt spectra are observed in all three reaction channels in coincidence with the delayed transitions. Additionally, the 769 keV transition is observed for the ^{97}Rb$(p, 2pn)^{95}$Kr channel. All transitions have a significance of $\approx 2\sigma$ or higher. Therefore, we tentatively propose new levels in ^{95}Kr, which correspond to the sum of these γ-ray transitions plus the energy of the known $(7/2)^+$ isomer. This will be compared to theory and discussed in Sec. IV.

IV. DISCUSSION

The experimental results provide new information about excited states and transition strengths. In this section, different theoretical predictions are discussed and compared with these results to further gain insight into the nuclear structure of ^{94,95,96}Kr.

A. The even-even ^{94,96}Kr

In Figs. 12 and 13 for ^{94}Kr and ^{96}Kr, respectively, experimentally obtained levels are compared to different theoretical calculations. The level structure in black (left) is obtained by using the five-dimensional collective Hamiltonian (5DCH) beyond-mean-field model [21] with the Gogny D1M interaction [41]. The level structure in blue (right) was adapted from constrained mean-field calculations [42], used to obtain microscopic energy surfaces, which in turn were used as input for a mapping procedure to determine the IBM Hamiltonian [18].

For ^{94}Kr, one can see that the experimental excitation energies for the lower yrast states are in good agreement with the 5DCH calculations, as is the $B(E2, 2^+ \rightarrow 0^+)$. The similarity to the 5DCH model could indicate that the excited state at 1217 keV, which decays into the 2^+_1 level and could have a

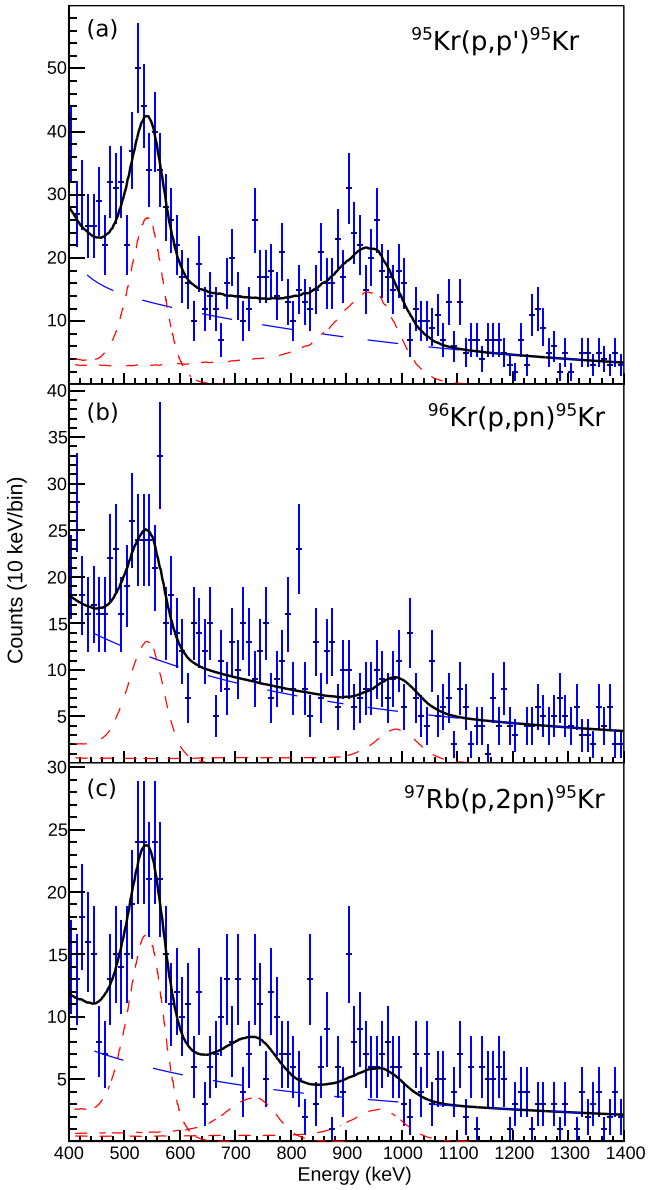

FIG. 11. Doppler-corrected γ-ray energy spectra measured with DALI2 for different reaction channels with an isomer gate on the delayed transitions measured with EURICA. The spectra were fitted with simulated response functions (red) and a two-component exponential background (blue dashed curve).

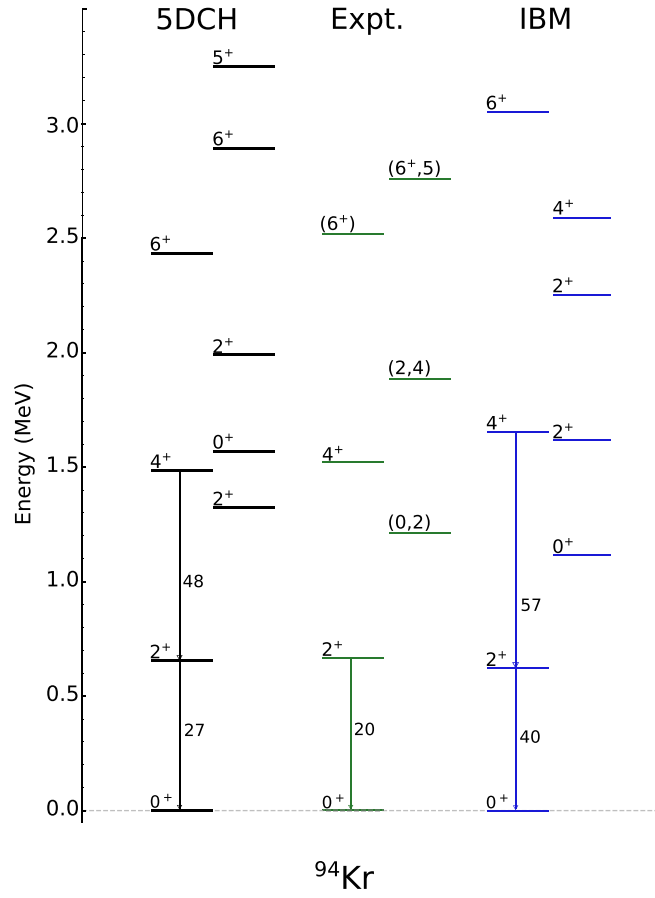

FIG. 12. Theoretical low-energy excitation levels of ^{94}Kr compared with experimental values [14,33]. Levels in black (left) were calculated using a 5DCH, in blue (right) using the mapped IBM [18]. $E2$ transition strengths in W.u. are shown along the arrows. See text for more details.

spin of 0 or 2, is in fact the 2_2^+ as predicted in that framework. The mapped IBM calculations predict a low-lying 0_2^+ level instead, which would be an indicator of a more pronounced shape coexistence. The similarity to the 5DCH calculations could also indicate that the 2786 keV state is a 6^+, with its energy lying close to the 6_2^+ level from the 5DCH calculations.

For ^{96}Kr, similarly to ^{94}Kr, the experimental values of the yrast levels are in better agreement with the 5DCH calculations, while the mapped IBM predicts generally higher energies (one exception is the 2_1^+). The low-lying (2_2^+) state at 888(16) keV is well reproduced by the 5DCH level structure, while the mapped IBM model does not predict any non-yrast level below the 4_1^+ state. The $E2$ transition strengths $B(E2, 2_2^+ \rightarrow 0^+)$ and $B(E2, 2_2^+ \rightarrow 2_1^+)$ are of the same order of magnitude for both models. When assuming a pure $E2$ transition for the $2_2^+ \rightarrow 2_1^+$ decay, the experimental limit derived from the $T_{1/2}$ is more consistent with the mapped IBM model.

In Fig. 14, the SCMF (β, γ)-deformation energy surfaces for ^{94,96}Kr are shown [18]. For $^{88-92}$Kr, these calculations show a pronounced γ softness [18], while a γ-soft oblate minimum appears in ^{94}Kr. For ^{96}Kr, the γ-softness is reduced and, next to the oblate ground state, a prolate local minimum develops at $\beta \approx 0.4$ which gets more pronounced for ^{98,100}Kr [18]. Experimentally, one would expect signs of a shape coexistence for ^{96}Kr in the manifestation of a low-lying 0_2^+ state as predicted by the 5DCH calculations. Even though this state was not observed, the similarity between experimentally observed and theoretically predicted states could suggest the existence of the low-lying 0_2^+ (see Fig. 13) and, thus, indicate an oblate-prolate shape coexistence appearing already in ^{96}Kr, which then becomes more pronounced in ^{98,100}Kr [16].

A recent study of octupole collectivity predicted increased octupole correlations for neutron-rich Kr isotopes at $N \approx 56$ [19]. The authors used constrained self-consistent

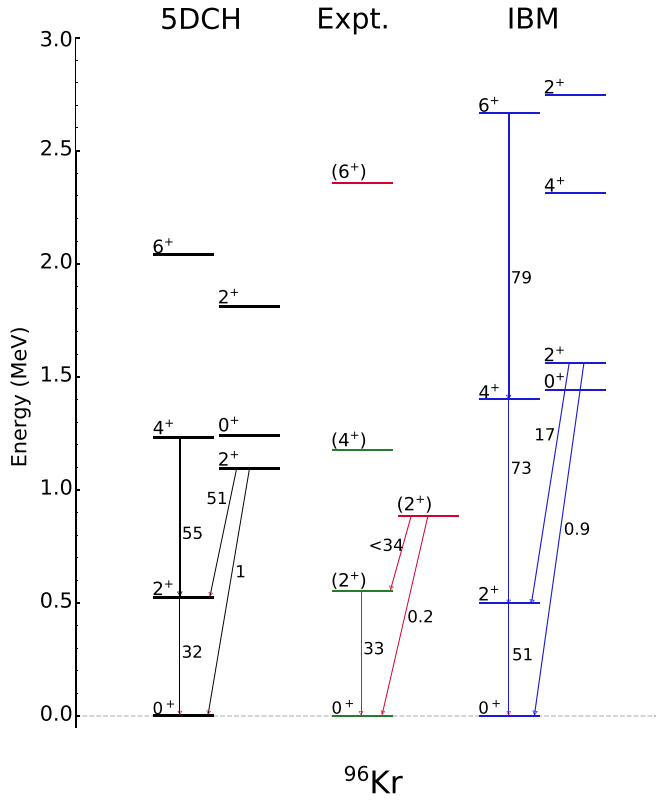

FIG. 13. Theoretical low-energy excitation levels of ^{96}Kr compared with experimental values. Levels in black (left) were calculated using a 5DCH, in blue (right) using the mapped IBM [18]. Levels in red were measured for the first time in this work. $E2$ transition strengths in W.u. are shown along the arrows [14]. See text for more details.

mean-field (SCMF) calculations based on the relativistic EDF, and the resulting SCMF potential energy surfaces in the (β_2, β_3) plane for ^{94,96}Kr are shown in Fig. 15 [19]. When going from 58 to 60 neutrons, a second shallow minimum develops on the prolate side and, more importantly, the depth of the octupole deformation on the prolate side is reduced. This explains the dramatic change in the predicted transition strength $B(E1, 3_1^- \rightarrow 2_1^+)$. Assuming theoretical transition probabilities, one can calculate a half-life of approximately

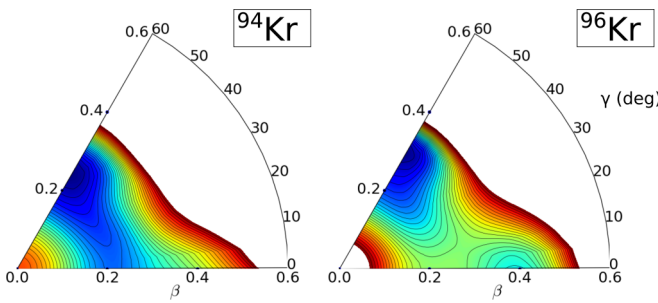

FIG. 14. SCMF (β, γ)-deformation energy surfaces for ^{94,96}Kr obtained with the Gogny-D1M EDF [18,41]. The energy difference between neighboring contours is 100 keV. See text for more details.

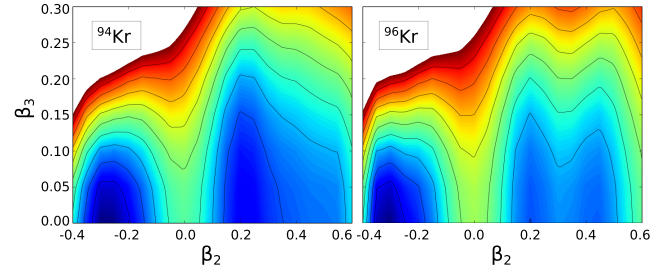

FIG. 15. SCMF (β_2, β_3) PESs for ^{94,96}Kr, calculated using the relativistic EDF. Contours join points on the surface with the same energy, and the difference between neighboring contours is 1 MeV [19].

0.015 ps for the 3_1^- state in ^{94}Kr and a lower limit of 120 ps for ^{96}Kr. Extracting half-lives from line-shape analysis is difficult for the (p, p') reaction channel since the reaction vertex cannot be reconstructed. Without the precise vertex reconstruction, the Doppler corrected peaks are broader, i.e., the half-lives deduced by line-shape analysis appear larger. Nevertheless, line-shape analysis of the $(3_1^-) \rightarrow 2_1^+$ transitions in ^{94,96}Kr as shown in Figs. 4 and 7 respectively yield half-lives of the same order of magnitude ($\approx$160 and $\approx$130 ps). Assuming similar broadening effects for both (p, p') reaction channels, one can deduce a change in transition probability, which qualitatively does not agree with the trend predicted by theory, since the expected change of several orders of magnitude in half-life was not observed.

B. The odd-A ^{95}Kr

In Fig. 16, the theoretical low-lying positive-parity excited levels of ^{95}Kr are shown [20] compared with previous experimental data [29,40] and new tentative levels suggested from this work. The theoretical structure of positive-parity levels was studied using a method where the constrained self-consistent mean-field approximation is used to compute single-particle energies and occupation probabilities for the odd-mass nuclei and deformation energy surfaces for neighboring even-even nuclei (based on the Gogny-D1M EDF) [20]. The interacting boson-fermion model (IBFM) Hamiltonian is then obtained using these values as microscopic input [43]. The missing parameters are obtained by fitting to experimental data for the isotope. Since only positive parity states have been calculated, only such were considered in the discussion below. The previously known excited levels are reproduced quite well by the theoretical calculations. We propose new tentative levels at 757(23), 965^{+30}_{-29}, and 1185^{+32}_{-34} keV, assuming single γ decays with the observed prompt γ-ray transitions of 561, 769, and 989 keV, which are feeding the known $(7/2)^+$ isomer (as shown in Sec. III C). Although no spin and parity can be firmly assigned, based on the γ decay selection rules, the observed feeding of the $(7/2)^+$ over the feeding of the $(3/2)^+$ and $(1/2)^+$ states below suggests possible spins in the range $9/2^+$ to $11/2^+$. From the theoretical levels in Fig. 16 at comparable energies, this would make the lowest $11/2^+$ and $9/2^+$ states plausible candidates. The

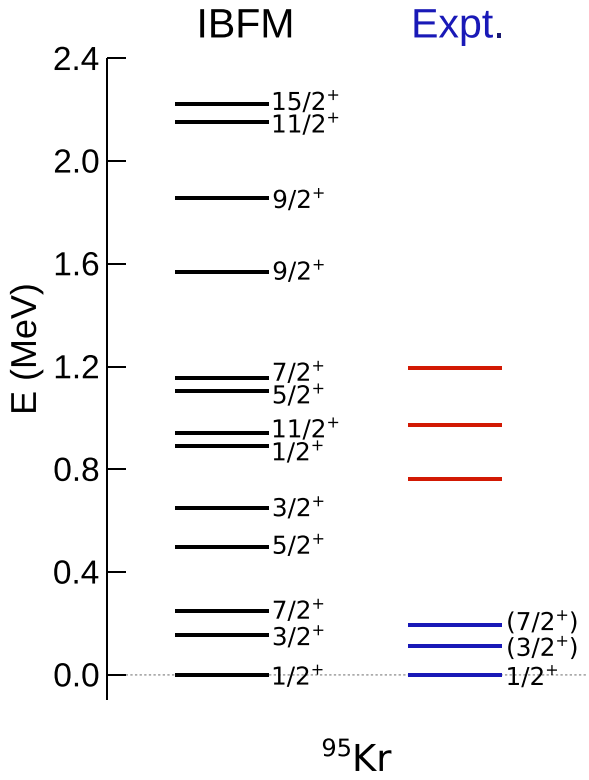

FIG. 16. Low-lying positive-parity excited states for ^{95}Kr on the left, predicted by the IBFM [20] compared with experimental data (on the right) from this work and Refs. [29,40]. The newly suggested excited levels decaying into the $(7/2^+)$ isomer are shown in red.

statistics for coincidences were limited, so no further levels could be placed in the level scheme.

V. CONCLUSIONS

We reported on the results of γ-ray spectroscopy of the neutron-rich isotopes ^{94,95,96}Kr. For ^{94,96}Kr, newly published results [15,33] could be confirmed. In both nuclei, several new transitions were observed. Non-yrast excited states and (3^-) candidates could be placed in the level schemes, which for ^{96}Kr was extended significantly. The experimental results were compared to mapped IBM and 5DCH calculations. The 5DCH model provides a good description of the excited states and some transition strengths in both nuclei, showing that for neutron-rich krypton isotopes already at $N = 60$ signs of the oblate-prolate shape coexistence are present. The lowering of the prolate structures is even more pronounced in ^{98,100}Kr as shown by the previous studies [16]. The new experimental results support the appearance of an oblate-prolate shape coexistence in ^{96}Kr. Thus, ^{94,96}Kr appear to be transitional nuclei between the spherical and γ-soft $N = 50$–56 and the stronger deformed $N = 62, 64$ krypton isotopes. In addition, the odd-A ^{95}Kr was studied, and several transitions were measured for the first time. Three transitions could be tentatively placed on top of the isomeric decay using delayed-prompt coincidences. In order to build a level scheme, future measurements with high resolution spectroscopy will be necessary.

ACKNOWLEDGMENTS

This work is supported by the Deutsche Forschungsgemeinschaft (DFG—German Research Foundation) under Grant No. BL 1513/1-1 and by the BMBF under Grants No. 05P15PKFNA, No. 05P19PKFNA, No. 05P15RDFN1, No. 05P19RDFN1, and No. 05P21RDFN1. We thank the RIKEN Nishina Centre accelerator staff and the BigRIPS team for providing the stable and high-intensity uranium beam and secondary beams, and the STFC (UK). J.P.E. thanks D. Regnier for useful discussions. The work of K. Nomura was supported by the Tenure Track Pilot Programme of the Croatian Science Foundation, the École Polytechnique Fédérale de Lausanne, and Project No. TTP-2018-07-3554, Exotic Nuclear Structure and Dynamics, with funds of the Croatian-Swiss Research Programme. B.D. and Z.L. were supported by the National Natural Science Foundation of China (Grants No. 12135004, No. 11635003, and No. 11961141004). R.T. was supported by JSPS Grant-in-Aid for JSPS Research Fellows JP14J08718.

[1] J. Wood, K. Heyde, W. Nazarewicz, M. Huyse, and P. van Duppen, Phys. Rep. **215**, 101 (1992).
[2] K. Heyde and J. L. Wood, Rev. Mod. Phys. **83**, 1467 (2011).
[3] F. Schussler, J. A. Pinston, E. Monnand, A. Moussa, G. Jung, E. Koglin, B. Pfeiffer, R. V. F. Janssens, and J. van Klinken, Nucl. Phys. A **339**, 415 (1980).
[4] T. A. Khan, W. D. Lauppe, K. Sistemich, H. Lawin, G. Sadler, and H. A. Selic, Z. Phys. A **283**, 105 (1977).
[5] E. Cheifetz, R. C. Jared, S. G. Thompson, and J. B. Wilhelmy, Phys. Rev. Lett. **25**, 38 (1970).
[6] F. K. Wohn, J. C. Hill, R. F. Petry, H. Dejbakhsh, Z. Berant, and R. L. Gill, Phys. Rev. Lett. **51**, 873 (1983).
[7] W. Urban *et al.*, Eur. Phys. J. A **22**, 241 (2004).
[8] C. Kremer, S. Aslanidou, S. Bassauer, M. Hilcker, A. Krugmann, P. vonNeumann-Cosel, T. Otsuka, N. Pietralla, V. Y. Ponomarev, N. Shimizu, M. Singer, G. Steinhilber, T. Togashi, Y. Tsunoda, V. Werner, and M. Zweidinger, Phys. Rev. Lett. **117**, 172503 (2016).
[9] E. Clément *et al.*, Phys. Rev. Lett. **116**, 022701 (2016).
[10] T. Togashi, Y. Tsunoda, T. Otsuka, and N. Shimizu, Phys. Rev. Lett. **117**, 172502 (2016).
[11] S. Naimi, G. Audi, D. Beck, K. Blaum, C. Bohm, C. Borgmann, M. Breitenfeldt, S. George, F. Herfurth, A. Herlert, M. Kowalska, S. Kreim, D. Lunney, D. Neidherr, M. Rosenbusch, S. Schwarz, L. Schweikhard, and K. Zuber, Phys. Rev. Lett. **105**, 032502 (2010).
[12] C. Sotty, M. Zielinska, G. Georgiev, D. L. Balabanski, A. E. Stuchbery, A. Blazhev, N. Bree, R. Chevrier, S. DasGupta, J. M. Daugas, T. Davinson, H. DeWitte, J. Diriken, L. P. Gaffney, K. Geibel, K. Hadynska-Klek, F. G. Kondev, J. Konki, T. Kroll, P. Morel, P. Napiorkowski, J. Pakarinen, P. Reiter, M. Scheck, M. Seidlitz, B. Siebeck, G. Simpson, H. Tornqvist, N. Warr, and F. Wenander, Phys. Rev. Lett. **115**, 172501 (2015).

[13] M. Albers *et al.*, Phys. Rev. Lett. **108**, 062701 (2012).
[14] M. Albers *et al.*, Nucl. Phys. A **899**, 1 (2013).
[15] J. Dudouet *et al.*, Phys. Rev. Lett. **118**, 162501 (2017).
[16] F. Flavigny *et al.*, Phys. Rev. Lett. **118**, 242501 (2017).
[17] T. R. Rodríguez, Phys. Rev. C **90**, 034306 (2014).
[18] K. Nomura, R. Rodríguez-Guzmán, Y. M. Humadi, L. M. Robledo, and H. Abusara, Phys. Rev. C **96**, 034310 (2017).
[19] K. Nomura, L. Lotina, T. Nikšić, and D. Vretenar, Phys. Rev. C **103**, 054301 (2021).
[20] K. Nomura, R. Rodríguez-Guzmán, and L. M. Robledo, Phys. Rev. C **97**, 064313 (2018).
[21] J. Libert, J.-P. Delaroche, and M. Girod, Eur. Phys. J. A **52**, 197 (2016).
[22] K. Nomura, N. Shimizu, and T. Otsuka, Phys. Rev. Lett. **101**, 142501 (2008).
[23] T. Kubo *et al.*, Prog. Theor. Exp. Phys. **2012**, 03C003 (2012).
[24] N. Fukuda, T. Kubo, T. Ohnishi, N. Inabe, H. Takeda, D. Kameda, and H. Suzuki, Nucl. Instrum. Methods Phys. Res. Sect. B **317**, 323 (2013).
[25] A. Obertelli *et al.*, Eur. Phys. J. A **50**, 8 (2014).
[26] S. Takeuchi, T. Motobayashi, Y. Togano, M. Matsushita, N. Aoi, K. Demichi, H. Hasegawa, and H. Murakami, Nucl. Instrum. Methods Phys. Res. Sect. A **763**, 596 (2014).
[27] S. Agostinelli *et al.*, Nucl. Instrum. Methods Phys. Res. Sect. A **506**, 250 (2003).
[28] P.-A. Söderström *et al.*, Nucl. Instrum. Methods Phys. Res. Sect. B **317**, 649 (2013).
[29] J. Genevey, R. Guglielmini, R. Orlandi, J. A. Pinston, A. Scherillo, G. Simpson, I. Tsekhanovich, N. Warr, and J. Jolie, Phys. Rev. C **73**, 037308 (2006).
[30] T. Rząca-Urban *et al.*, Eur. Phys. J. A **9**, 165 (2000).
[31] M. Lebois, N. Jovančević, D. Thisse, R. Canavan, D. Étasse, M. Rudigier, and J. N. Wilson, Nucl. Instrum. Methods Phys. Res., Sect. A **960**, 163580 (2020).
[32] N. Jovančević *et al.*, Acta Phys. Pol. B **50**, 297 (2019).
[33] R.-B. Gerst *et al.*, Phys. Rev. C **102**, 064323 (2020).
[34] V. Vaquero, A. Jungclaus, P. Doornenbal, K. Wimmer, A. Gargano, J. A. Tostevin, S. Chen, E. Nacher, E. Sahin, Y. Shiga, D. Steppenbeck, R. Taniuchi, Z. Y. Xu, T. Ando, H. Baba, F. L. Garrote, S. Franchoo, K. Hadynska-Klek, A. Kusoglu, J. Liu, T. Lokotko, S. Momiyama, T. Motobayashi, S. Nagamine, N. Nakatsuka, M. Niikura, R. Orlandi, T. Saito, H. Sakurai, P. A. Soderstrom, G. M. Tveten, Z. Vajta, and M. Yalcinkaya, Phys. Rev. Lett. **118**, 202502 (2017).
[35] V. Vaquero, A. Jungclaus, P. Doornenbal, K. Wimmer, A. M. Moro, K. Ogata, T. Furumoto, S. Chen, E. Nacher, E. Sahin, Y. Shiga, D. Steppenbeck, R. Taniuchi, Z. Y. Xu, T. Ando, H. Baba, F. L. BelloGarrote, S. Franchoo, K. Hadynska-Klek, A. Kusoglu, J. Liu, T. Lokotko, S. Momiyama, T. Motobayashi, S. Nagamine, N. Nakatsuka, M. Niikura, R. Orlandi, T. Y. Saito, H. Sakurai, P. A. Soderstrom, G. M. Tveten, Z. Vajta, and M. Yalcinkaya, Phys. Rev. C **99**, 034306 (2019).
[36] T. Kibédi and R. Spear, At. Data Nucl. Data Tables **80**, 35 (2002).
[37] D. Hofer *et al.*, Nucl. Phys. A **551**, 173 (1993).
[38] S. Matsuki, N. Sakamoto, K. Ogino, Y. Kadota, Y. Saito, T. Tanabe, M. Yasue, and Y. Okuma, Phys. Lett. B **72**, 319 (1978).
[39] L. A. Riley, M. L. Agiorgousis, T. R. Baugher, D. Bazin, M. Bowry, P. D. Cottle, F. G. DeVone, A. Gade, M. T. Glowacki, K. W. Kemper, E. Lunderberg, D. M. McPherson, S. Noji, F. Recchia, B. V. Sadler, M. Scott, D. Weisshaar, and R. G. T. Zegers, Phys. Rev. C **90**, 011305(R) (2014).
[40] D. Kameda *et al.*, Phys. Rev. C **86**, 054319 (2012).
[41] S. Goriely, S. Hilaire, M. Girod, and S. Péru, Phys. Rev. Lett. **102**, 242501 (2009).
[42] P. Ring and P. Schuck, *The Nuclear Many-Body Problem*, (Springer-Verlag, Berlin, 1980).
[43] K. Nomura, T. Nikšić, and D. Vretenar, Phys. Rev. C **93**, 054305 (2016).